Mon. Not. R. Astron. Soc. **000**, 8–?? (2002) Printed 7 January 2014 (MN LATEX style file v2.2)

The prompt-early afterglow connection in gamma-ray bursts: implications for the early afterglow physics

R. Hascoët[1⋆], F. Daigne[2] and R. Mochkovitch[2⋆]
[1]*Physics Department and Columbia Astrophysics Laboratory, Columbia University, 538 West 120th Street, New York, NY 10027, USA.*
[2]*UPMC-CNRS, UMR7095, Institut d'Astrophysique de Paris, F-75014, Paris, France.*

arXiv:1401.0751v1 [astro-ph.HE] 3 Jan 2014

Accepted **.**.**. Received **.**.**; in original form **.**.**

ABSTRACT
The early X-ray afterglow of gamma-ray bursts revealed by *Swift* carried many surprises. Following an initial steep decay the light-curve often exhibits a plateau phase that can last up to several 10^4 s, with in addition the presence of flares in 50% of the cases. We focus in this paper on the plateau phase whose origin remains highly debated. We confront several newly discovered correlations between prompt and afterglow quantities (isotropic emitted energy in gamma-rays, luminosity and duration of the plateau) to several models proposed for the origin of plateaus in order to check if they can account for these observed correlations. We first show that the scenario of plateau formation by energy injection into the forward shock leads to an efficiency crisis for the prompt phase and therefore study two possible alternatives: the first one still takes place within the framework of the standard forward shock model but allows for a variation of the microphysics parameters to reduce the radiative efficiency at early times; in the second scenario the early afterglow results from a long-lived reverse shock. Its shape then depends on the distribution of energy as a function of Lorentz factor in the ejecta. In both cases, we first present simple analytical estimates of the plateau luminosity and duration and then compute detailed light curves. In the two considered scenarios we find that plateaus following the observed correlations can be obtained under the condition that specific additional ingredients are included. In the forward shock scenario, the preferred model supposes a wind external medium and a microphysics parameter ϵ_e that first varies as $n^{-\nu}$ (n being the external density), with $\nu \sim 1$ to get a flat plateau, before staying constant below a critical density n_0. To produce a plateau in the reverse shock scenario the ejecta must contain a tail of low Lorentz factor with a peak of energy deposition at $\Gamma \gtrsim 10$.

Key words: Gamma rays bursts: general; Radiation mechanisms: non-thermal; Shock waves.

1 INTRODUCTION

Before the launch of the *Swift* satellite (Gehrels et al. 2004) the afterglow was believed to be the best understood part of GRB physics, being explained by the energy dissipated in the forward shock formed by the jet impacting the burst environment (Meszaros & Rees 1997; Sari et al. 1998). However, the many surprises of the early X-ray afterglow revealed by *Swift* - initial steep decay, plateau phase, flares - have considerably complicated the picture (Nousek et al. 2006; O'Brien et al. 2006).

Several mechanisms have been proposed to explain the plateau, the most popular being energy injection into the forward shock (Rees & Meszaros 1998; Sari & Mészáros 2000; Nousek et al. 2006) resulting from a long-lasting activity of the central engine (which could be also responsible for the flares, Zhang et al. 2006) or from a wide distribution of Lorentz factors in the ejecta. Other possibilities include *(i)* direct emission from a magnetar (e.g. Rowlinson et al. 2013), *(ii)* coasting of the external blastwave in a wind medium (e.g. Shen & Matzner 2012), *(iii)* varying microphysics parameters (Granot et al. 2006; Ioka et al. 2006), *(iv)* reverse shock contribution (Genet et al. 2007; Uhm & Beloborodov 2007). In *(i)* the end of the plateau corresponds to the spindown time of the protomagnetar or its collapse to a blackhole. Therefore this scenario is mostly promising to explain peculiar plateaus that are followed by a steep decay (temporal index ~ -2 or steeper), while "standard" plateaus (followed by a temporal decay index ~ -1.5) are most likely of afterglow origin; *(ii)* requires the Lorentz factor of the ejecta to be at most a few tens (so that the coasting phase lasts long enough), which is in severe tension with the minimum Lorentz factor of the ejecta derived from the compactness constraint (e.g. Lithwick & Sari 2001; Hascoët et al. 2012). In the present work we focus on cases *(iii)* and *(iv)* in connection with the recent discovery of correlations between prompt and afterglow quantities (Dainotti et al. 2011; Margutti et al. 2013; Dainotti et al. 2013; Grupe et al. 2013). We especially want to ex-

⋆ E-mail: hascoet@astro.columbia.edu

plore if these correlations can be satisfied by the models and which kind of constraints do they impose.

We first summarize in Sect. 2 the observational results on the prompt-afterglow correlations and in Sect. 3 we show that explaining the plateau by late energy injection into the forward shock leads to an "efficiency crisis" for the prompt phase. We then consider in Sect. 4 the possibility that the microphysics parameters in the forward shock vary during the early afterglow and in Sect. 5 we explore the alternative model where the afterglow is made by the reverse shock. Our results are discussed in Sect. 6, which is also the conclusion.

2 THE PROMPT AFTERGLOW CONNECTION

For events with a measured redshift and a well-defined plateau phase, quantities such as $t_{\rm p}$ – duration of the plateau in the burst rest frame, $L_{\rm P}$ – luminosity at the end of the plateau or $E_{\rm X}$ – energy released in X-rays during the plateau, can be measured together with the isotropic energy in gamma-rays of the prompt phase $E_{\gamma,\rm iso}$. From the samples recently analyzed by Dainotti et al. (2011), Margutti et al. (2013) and Dainotti et al. (2013) some clear correlations appear between prompt and afterglow quantities. The plateau luminosity $L_{\rm p}$ and energy E_X increase with $E_{\gamma,\rm iso}$ and decrease for larger $t_{\rm p}$. Since an increase of $L_{\rm p}$ and E_X with $E_{\gamma,\rm iso}$ could be expected, we also consider below the ratios $L_{\rm p}/E_{\gamma,\rm iso}$ and $E_X/E_{\gamma,\rm iso}$, which respectively decreases and barely evolves with increasing $t_{\rm p}$.

These prompt-afterglow correlations represent potentially important clues to understand the many surprises of the early afterglow. In the standard forward shock scenario (for a wide range of parameters) the X-ray flux depends on the energy injected into the shock and the microphysics, but not on the density of external medium. In the reverse shock scenario the shape of the early afterglow depends both on the density of the burst environment and on the distribution of energy in the ejecta that is crossed by the reverse shock. Below, we investigate under which conditions the observed correlations can be reproduced in the framework of these two scenarios.

3 MAKING A PLATEAU WITH LATE ENERGY INJECTION

Continuous energy injection into the forward shock (Rees & Meszaros 1998; Sari & Mészáros 2000; Nousek et al. 2006) is commonly invoked to account for plateau formation. For the most extended plateaus it however imposes to inject up to several hundreds times the energy that was initially present to power the prompt phase. This is illustrated in Fig. 1 where we have plotted X-ray light curves all with the same initial injected energy $E_0 = 10^{52}$ erg but where the final energy is 2, 10 or 100 times larger. It is only in this last case that a plateau lasting several hours can be obtained. Energy injection into the forward shock can take place in two ways: either the source stays active during the whole duration of the plateau or it is short-lived but has produced a tail of low Lorentz factor material that is progressively catching up, adding energy to the shock. We have considered this latter case to obtain Fig.1 (the source being active for 10 s) but the former one gives similar results.

The huge amount of energy to be injected after the end of the prompt phase leads to an "efficiency crisis" for the prompt mechanism. The measured gamma-ray efficiency is

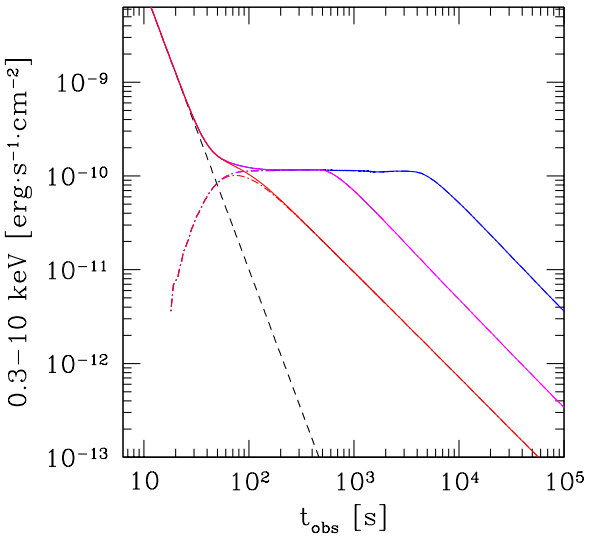

Figure 1. X-ray afterglow light curves from late energy injection into the forward shock. The initial energy in the shock is $E_0 = 10^{52}$ erg and the red, purple and blue light curves respectively correspond to a final energy being respectively 2, 10 and 100 times larger. The dashed line represents the continuation of the early steep decay that terminates the prompt emission, while the dashed-dotted line shows the forward shock emission only. A redshift $z = 1$, a uniform external medium of density $n = 10$ cm^{-3}, and constant microphysics parameters $\epsilon_e = 0.1$ and $\epsilon_B = 0.01$ have been assumed.

$$f_{\gamma,\rm mes} = \frac{E_\gamma}{E_\gamma + E_{\rm fs}} \tag{1}$$

where the energy in the forward shock, $E_{\rm fs}$, is estimated from multiwavelength fits of the afterglow typically after one day (i.e. after energy injection; see e.g. Zhang et al. 2007). However the true efficiency is

$$f_{\gamma,\rm true} = \frac{E_\gamma}{E_\gamma + E_{\rm fs,0}} = \frac{1}{1 + \frac{1}{k}\left(\frac{1}{f_{\gamma,\rm mes}} - 1\right)} \tag{2}$$

where $E_{\rm fs,0}$ is the energy initially present in the forward shock and $k = E_{\rm fs}/E_{\rm fs,0} \gg 1$. With for example $f_{\gamma,\rm mes} = 0.1$, the true efficiency is $f_{\gamma,\rm true} = 0.53$ for $k = 10$ and 0.92 for $k = 100$. These values of $f_{\gamma,\rm true}$ seems unreachable for any of the proposed prompt mechanisms: the efficiency of internal shocks can barely reach 10% (e.g. Rees & Meszaros 1994; Kobayashi et al. 1997; Daigne & Mochkovitch 1998) while that of comptonized photosphere (e.g. Rees & Mészáros 2005; Beloborodov 2010) or reconnection (e.g. Spruit et al. 2001; Drenkhahn & Spruit 2002) models is more uncertain but certainly cannot exceed 50%.

4 MAKING A PLATEAU AVOIDING AN ENERGY CRISIS

4.1 Forward shock scenario

The standard forward shock scenario can successfully account for the afterglow evolution after about one day but fails to reproduce the plateau phase. A backwards extrapolation of the late afterglow flux lies above the plateau, which might therefore be interpreted as the indication that some normally expected radiation is "missing". This can be the case if the radiative efficiency of the forward shock

during the early afterglow is smaller than assumed by the simplest version of the standard model. The most obvious way to reduce the efficiency is to relax the assumption that the microphysics parameters stay constant throughout the whole afterglow evolution (Granot et al. 2006; Ioka et al. 2006).

For both a uniform and a wind external medium the afterglow X-ray flux behaves as (Panaitescu & Kumar 2000)

$$F_{\rm X} \propto E^{\frac{p+2}{4}} \epsilon_e^{p-1} \epsilon_B^{\frac{p-2}{4}} t^{-\frac{3p-2}{4}} \quad (3)$$

where E is the burst isotropic energy, ϵ_e and ϵ_B the microphysics parameters and p the power-law index of the accelerated electron spectrum. Eq. (3) is valid as long as the X-ray frequency is larger than both the injection and cooling frequencies, which is generally the case.

With $2 < p < 3$ the dependence on ϵ_B is weak so that in practice only playing with ϵ_e can really affect the flux evolution. A priori ϵ_e can be a function of the shock Lorentz factor, the density of the external medium (in the case of a stellar wind) or both. The stellar wind case is of special interest if we make the simple assumption that, below a critical density n_0, ϵ_e is constant while $\epsilon_e \propto n^{-\nu}$ (with $\nu > 0$) for $n > n_0$. Since the density seen by the forward shock is given by

$$n(t) \simeq \frac{4\pi c}{m_p} \frac{A^2}{E\, t} \simeq 5.6\, 10^2 A_*^2 E_{53}^{-1} t_3^{-1} \ {\rm cm}^{-3} \quad (4)$$

where t is the (redshift-corrected) observer time and A_* is the wind density normalization ($\rho(r) = A/R^2$ with $A = 5 \times 10^{11} A_*$ g cm^{-1}) the transition at n_0, which marks the end of the plateau, takes place at

$$t_{\rm p} \approx 5.6\, 10^5 A_*^2 n_0^{-1} f_\gamma E_{\gamma,53}^{-1} \ {\rm s} \quad (5)$$

where f_γ is the gamma-ray efficiency of the prompt phase and $E_{\gamma,53}$ is the isotropic gamma-ray energy release. Then, if the product $A_*^2 n_0^{-1} f_\gamma$ typically stays in the range $3 \times 10^{-4} - 3 \times 10^{-2}$ the resulting $[t_{\rm p}, E_{\gamma,{\rm iso}}]$ sequence can accommodate most of the bursts in the Margutti et al. (2013) sample (see Fig. 5).

A flat plateau is expected for

$$\nu = \nu_0 = \frac{3p-2}{4(p-1)} = 1 - \frac{p-2}{4(p-1)} \approx 1 \quad (6)$$

while for $\nu < \nu_0$ (resp. $\nu > \nu_0$) the plateau flux is decreasing (resp. rising) with time.

With $\epsilon_e \propto n^{-1}$ and from Eq. (3), a flat plateau extending over two decades in time requires an increase of ϵ_e by a factor of about 100 from the beginning to the end of the plateau. It is beyond the scope of this paper to decide if this is indeed possible but it is remarkable that acting on one single parameter can lead to the formation of a plateau that also satisfies the observed prompt-afterglow correlations (see §5.1).

The other possibility where ϵ_e depends on the Lorentz factor does not yield satisfactory results. Assuming that the transition from a varying to a constant ϵ_e takes place at a fixed Γ, the deceleration laws of the blast wave

$$\Gamma \propto \begin{cases} \left(\frac{E}{n}\right)^{1/8} t^{-3/8} & \text{uniform medium} \\ \left(\frac{E}{A}\right)^{1/4} t^{-1/4} & \text{wind} \end{cases} \quad (7)$$

then lead to $t_p \propto E_\gamma^{1/3}$ and $t_p \propto E_\gamma$ in the uniform medium and wind cases respectively, showing a trend opposite to the observed one.

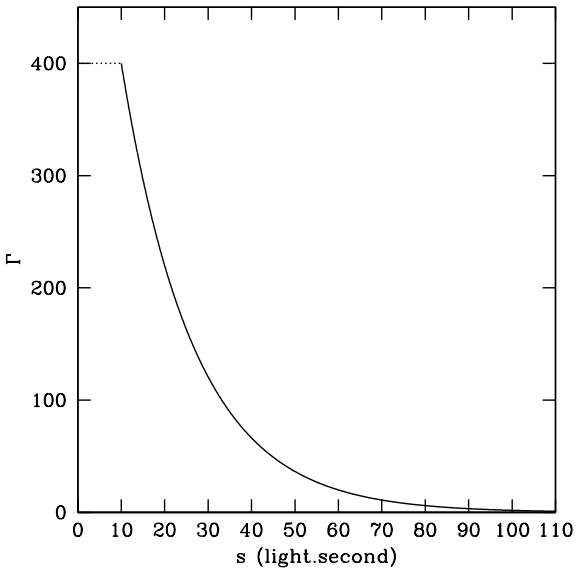

Figure 2. Lorentz factor in the ejecta as a function of the distance from the front (in light.seconds). The "head" (from 0 to 10 light.seconds) is made of material with typical Lorentz factor $\overline{\Gamma} = 400$ while in the tail Γ decreases from 400 to unity following Eq. (8), so that $\frac{dE}{d{\rm Log}\Gamma}$ is constant.

4.2 Reverse shock scenario

We now suppose that the ejecta emitted by the central engine is made of a "head" with material at high Lorentz factors ($\Gamma \sim 10^2$ - 10^3), followed by a "tail" where the Lorentz factor decreases to much smaller values, possibly close to unity. The head is responsible for the prompt emission while the reverse shock propagating through the tail makes the afterglow.

We adopt for the head a constant energy injection rate $\dot{E}_{\rm H}$ for a duration of 10 s. We do not specify the distribution of the Lorentz factor and simply consider its average value, supposed to be $\overline{\Gamma} = 400$. The tail that follows lasts for 100 s but this value is not critical as long as it remains sufficiently short not to exceed the duration of the early steep decay phase observed at the beginning of most X-ray light curves. We start with a simple case where the distribution of energy in the tail $\frac{dE}{d{\rm Log}\Gamma}$ is constant from $\Gamma = 400$ to $\Gamma = 1$. This can be obtained by adopting a constant energy injection rate $\dot{E}_{\rm T}$ and a Lorentz factor of the form

$$\Gamma_{\rm T}(s) = 400^{1.1 - s/(c \times 100{\rm s})} \ , \quad (8)$$

from $s = 10$ to 110 light.seconds, the distance s being counted from the front to the back of the flow (see Fig. 2).

Using the methods described in Genet et al. (2007) we have obtained the power $P_{\rm diss}(t)$ dissipated by the reverse shock as a function of arrival time to the observer for $\dot{E}_{\rm H} = 10\dot{E}_{\rm T} = 5\, 10^{52}$ erg.s^{-1} (so that equal amounts of energy are injected in the head and tail) and two possibilities for the burst environment: (*i*) a uniform medium with $n = 1000$ cm^{-3} (supposed to be representative of a massive star environment) or (*ii*) a stellar wind with a wind parameter $A_* = 1$. Going from the dissipated power to actual light curves depends on the assumptions that have to be made for the microphysics parameters. The general shape of the early X-ray afterglow light curves however remains globally similar to the evolution of $P_{\rm diss}(t)$ so that some conclusions can already be reached without having to consider the uncertain post-shock microphysics.

Fig. 3 (red and blue curves) shows that if energy is evenly distributed in the tail (constant $\frac{dE}{d\mathrm{Log}\Gamma}$) the dissipated power approximately decays as t^{-1} after about 1000 s, for both a uniform and a wind ambient medium. The contrast $\kappa = \Gamma/\Gamma_{\rm bw}$, where Γ and $\Gamma_{\rm bw}$ are respectively the Lorentz factors of the unshocked ejeta and the blastwave, is larger for the uniform medium than for the wind case ($\kappa \simeq 2$ and $\sqrt{2}$ respectively, see Genet et al. 2007). As seen in Fig. 3 the dissipated power is therefore larger (by a factor $3-5$) in the uniform medium.

We now vary the energy deposition in the tail, concentrating more power at some value of the Lorentz factor. We have for example considered a simple model where

$$\dot{E}_{\rm T}(\Gamma) = \begin{cases} \dot{E}_* \left(\frac{\Gamma}{\Gamma_*}\right)^{-q} & \text{for } \Gamma > \Gamma_* \\ \dot{E}_* \left(\frac{\Gamma}{\Gamma_*}\right)^{q'} & \text{for } \Gamma < \Gamma_* \end{cases} \tag{9}$$

the value of $\dot{E}_*$ being fixed by the total energy injected in the tail. Figures 3a and 3b respectively show the dissipated power for $\Gamma_* = 12$, $q = q' = 1.5$ and 2.5 (uniform medium) and $\Gamma_* = 20$, $q = q' = 3$ and 4.5 (stellar wind) with $E_{\rm H} = E_{\rm T}$ in both cases. When energy deposition is more concentrated (increasing q and q') a plateau progressively forms and becomes flatter. The value of Γ_* in Eq. (9) fixes the duration of the plateau as it corresponds to the time when the reverse shock reaches s_* where $\Gamma_{\rm T}(s_*) = \Gamma_*$. The q parameter controls the flatness of the plateau while q' controls the decay index after the plateau.

The duration $t_{\rm p}$ of the plateau is roughly given by

$$t_{\rm p} \sim \begin{cases} 6\times 10^5 E_{\rm H,53}^{1/3} n^{-1/3} \Gamma_{*,1}^{-8/3} \ {\rm s} \\ 10^5 \, E_{\rm H,53} \, A_*^{-1} \, \Gamma_{*,1}^{-4} \ \ {\rm s} \end{cases} \tag{10}$$

for a uniform and wind medium respectively. Eq. (10) corresponds to the situation of a decelerating shell that does not receive any supply of energy, contrary to the present case where material from the tail is continuously catching up. It however remains approximately correct as long as $E_{\rm T}$ does not largely exceeds the energy $E_{\rm H}$ in the head of the ejecta (as it happens in models where the plateau is made by energy injection into the forward shock discussed in Sect. 3).

An analytical solution corresponding to the results of Fig. 3 can be obtained from the following expression of $P_{\rm diss}$ (Genet et al, 2007)

$$P_{\rm diss} = \frac{dM}{d\Gamma}\frac{d\Gamma}{dt}\Gamma e c^2 \ , \tag{11}$$

where $M(\Gamma)$ gives the distribution of mass as a function of the Lorentz factor in the tail, $\Gamma(t)$ is the Lorentz factor of the tail material just being shocked at observer time t (without the $(1+z)$ time dilation factor) and e is the fraction of the incoming material kinetic energy dissipated in the reverse shock. From Eq. (9) we get

$$\frac{dM}{d\Gamma} = \frac{\dot{E}_*}{\Gamma_* c^3}\left(\frac{\Gamma}{\Gamma_*}\right)^{\pm q-1}\frac{ds}{d\Gamma} = \frac{\dot{E}_*\tau}{\Gamma_* c^2}\left(\frac{\Gamma}{\Gamma_*}\right)^{\pm q-1}\times\frac{1}{\Gamma} \ , \tag{12}$$

with $\tau = 100/\ln 400$ s (we do not distinguish between q and q' in Eq. (12) to simplify the notation). The total energy in the tail is given by

$$E_{\rm T} \ = \ \int_{10}^{110} \dot{E}_{\rm T}\, dt = \dot{E}_*\tau\times\varphi_{qq'} \ , \tag{13}$$

with

$$\varphi_{qq'} = \frac{1}{q}+\frac{1}{q'} \ . \tag{14}$$

We now write $\Gamma(t)$ as

$$\Gamma(t) \simeq \Gamma_*\left(\frac{t}{t_{\rm p}}\right)^{-\gamma} \ , \tag{15}$$

with $\gamma = 3/8$ (resp. $1/4$) for a uniform medium (resp. a stellar wind) and with $t_{\rm p}$ being the duration of the plateau. Then, combining Eqs (11-12-13-15) and the expression of e

$$e = \frac{1}{2}\left[1-(1-2\gamma)^{1/2}\right]^2 \ , \tag{16}$$

(Genet et al, 2007) we finally obtain

$$P_{\rm diss}(t) = \frac{E_{\rm T}}{t_{\rm p}\,\varphi_{qq'}}F(\gamma)\left(\frac{t}{t_{\rm p}}\right)^{\pm q\gamma-1} \ , \tag{17}$$

with

$$F(\gamma) = \frac{\gamma}{2}\left[1-(1-2\gamma)^{1/2}\right]^2 \ . \tag{18}$$

The decay indices before and after the break at the end of the plateau are

$$\begin{cases} \alpha_1 = \gamma q - 1 \\ \alpha_2 = -\gamma q' - 1 \end{cases} \tag{19}$$

so that a flat plateau is expected for $q = 1/\gamma$ (i.e. $q = 8/3$ and 4 in the uniform medium and wind cases respectively). For the examples shown in Fig. 3, Eq. (19) gives $\alpha_1 = -7/16$ and $-1/16$ for $q = 1.5$ and 2.5 (uniform medium) and $\alpha_1 = -1/4$ and $1/8$ for $q = 3$ and 4.5 (wind). If we impose a decay index $\alpha_2 = -1.5$ after the plateau we get the condition $q' = 1/2\gamma$ (i.e. $q' = 4/3$ and 2 for the uniform medium and wind cases respectively). With our simple choice of $q = q'$ in Fig. 3 the decay is steeper when the plateau is flatter.

5 BUILDING A SEQUENCE OF MODELS

5.1 Forward shock scenario

It has been shown in Sect. 4.1 that a transition in the behavior of ϵ_e (from rising to constant) at a fixed density n_0 marks the end of the plateau at a time $t_{\rm p}$ given by Eq. (5). The X-ray luminosity $L_{\rm p}$ at $t = t_{\rm p}$ then writes from Eqs.(3) and (4)

$$L_{\rm p} \propto E^{\frac{p+2}{4}} t_{\rm p}^{-\frac{3p-2}{4}} \propto t_{\rm p}^{-p} \propto E_{\gamma,{\rm iso}}^{p} \tag{20}$$

as long as the microphysics parameters at the end of the plateau and the gamma-ray efficiency do not vary much from burst to burst. Fig. 4a shows a sequence of afterglow light curves corresponding to different values of the isotropic gamma-ray energy release and the following choice of parameters: $\epsilon_e = 0.1\,(n/n_0)^{-1}$ for $n > n_0 = 15$ cm^{-3} and $\epsilon_e = 0.1$ for $n < n_0$, $A_* = 0.5$, $p = 2.2$, $f_\gamma = 0.2$. It was obtained with a detailed calculation where the evolution of each elementary shocked shell is considered separately (Beloborodov 2005) except for the pressure, which is uniform throughout the whole shocked ejecta. The electron population and magnetic field of each newly shocked shell are computed taking into account the corresponding shock physical conditions and microphysics parameters. Then, each electron population is followed individually during the whole evolution, starting from the moment of injection, and taking into account radiative and adiabatic cooling. The resulting light curves somewhat differ from the simple analytical prediction of Sect.4.1. The plateaus do not stay all flat, the brightest ones being slowly rising.

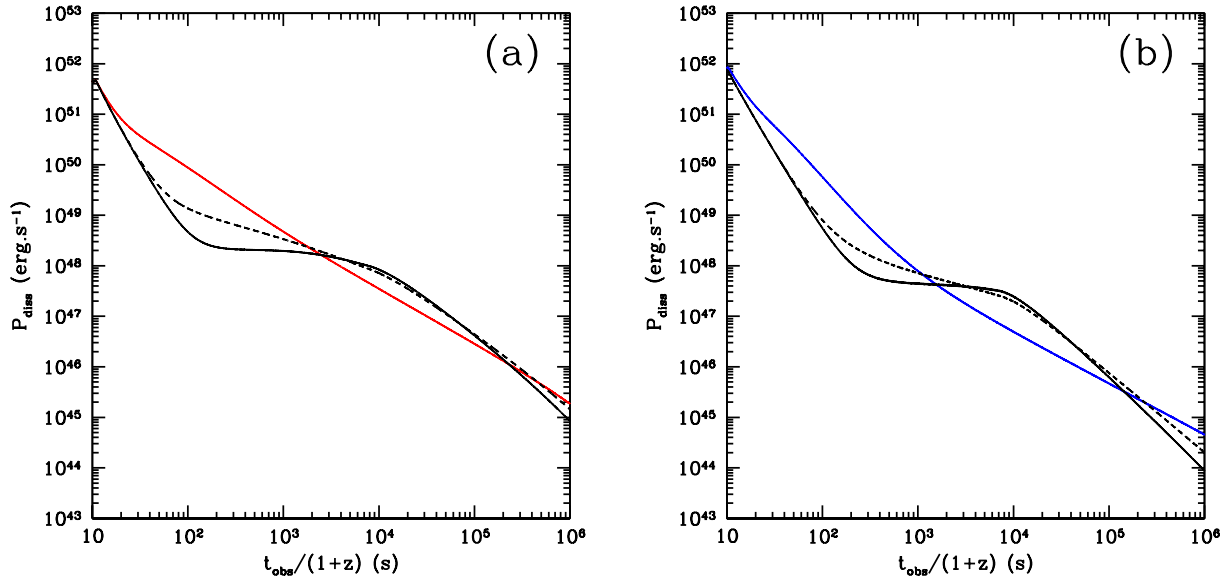

Figure 3. Dissipated power in the reverse shock as a function of observer time for equal amounts of energy $E_{\rm H} = E_{\rm T} = 5\,10^{53}$ erg in the head and tail. The distribution of energy in the tail as a function of Lorentz factor is given by Eq. (9). (a): Uniform external medium of density $n = 1000$ cm^{-3}, $\Gamma_* = 12$, $q = q' = 1.5$ (dashed line) and $q = q' = 2.5$ (full line); (b): stellar wind with $A_* = 1$, $E_{\rm H} = E_{\rm T} = 5\,10^{53}$ erg, $\Gamma_* = 20$, $q = q' = 3$ (dashed line) and $q = q' = 4.5$ (full line). The red and blue lines have $q = q' = 0$ and correspond to a uniform distribution of energy $\frac{dE}{d{\rm Log}\Gamma}$ in the tail.

5.2 Reverse shock scenario

Using Eq. (10) it is possible to link the duration of the plateau to the gamma-ray energy release $E_{\gamma,\rm iso}$ if Γ_* depends on the burst energy. A relation $\Gamma_{\rm H} \propto E_{\gamma,\rm iso}^{1/2}$ is suggested from the work of Liang et al. (2010) and Ghirlanda et al. (2012) based on the rising time of the optical light curve, but Hascoet et al. (2013) have shown that it partially results from selection effects and has an intrinsic scatter much larger than originally inferred. Nevertheless we adopt $\Gamma_* \propto E_{\gamma,\rm iso}^{1/2}$ for simplicity, keeping in mind a potential large dispersion, see §5.3 below. If moreover the gamma-ray efficiency

$$f_\gamma = \frac{E_{\gamma,\rm iso}}{E_{\rm H}} \tag{21}$$

does not vary much from burst to burst, we obtain

$$t_{\rm p} \propto E_{\rm H}^{-1} \propto E_{\gamma,\rm iso}^{-1} \tag{22}$$

for both a uniform medium and a stellar wind. Together with Eq. (17) this fixes the dissipated power during the plateau phase

$$P_{\rm diss} \propto t_{\rm p}^{-2} \propto E_{\gamma,\rm iso}^{2}\ . \tag{23}$$

To now compute a sequence of X-ray light curves from the dissipated power we have to fix the microphysics parameters ϵ_e and ϵ_B in the shocked material for which we adopt the fiducial values $\epsilon_e = 0.1$ $\epsilon_B = 0.01$. The results for a uniform external medium of density $n = 1000$ cm^{-3} are shown in Fig. 4b. They were obtained with the same method of calculation used in the forward shock case and outlined in Sect.5.1. We start with a model having $E = E_{\rm H} = E_{\rm T} = 2\,10^{54}$ erg, $\Gamma_* = 16$, $q = 8/3$ and $q' = 4/3$ and then construct the sequence by multiplying or dividing $E_{\rm H}$ and $E_{\rm T}$ by a the same factor F (i.e. we keep $E_{\rm H} = E_{\rm T}$) and simultaneously $\Gamma_{\rm H}$ and $\Gamma_{\rm T}$ by $F^{1/2}$. This prescription corresponds to $\Gamma_* = \Gamma_0 E_{\rm iso,53}^{1/2}$ with $\Gamma_0 = 35$. The sequence obtained for a stellar wind is similar, but due to the smaller contrast in Lorentz factor at the shock, the plateau flux is about 3 times smaller for the same value of the injected energy.

5.3 Prompt-afterglow correlations

When the sequences obtained in the previous section are transported back into the burst rest frame, the predicted correlations linking the plateau duration $t_{\rm p}$, luminosity $L_{\rm p}$, energy release in X-rays E_X and the isotropic gamma-ray energy $E_{\gamma,\rm iso}$ can be compared to data. This is done in Fig. 5 for the $[L_{\rm p}, E_{\gamma,\rm iso}]$, $[t_{\rm p}, E_{\gamma,\rm iso}]$, $[L_{\rm p}, t_{\rm p}]$, $[L_{\rm p}/E_{\gamma,\rm iso}, t_{\rm p}]$, $[E'_X, E_{\gamma,\rm iso}]$ and $[E'_X/E_{\gamma,\rm iso}, t_{\rm p}]$ relations. Since the plateaus in observed bursts are not all flat contrary to our synthetic ones, we have replaced, for a simple comparison between data and models, the true X-ray energy release by the product $E'_{\rm X} = L_{\rm p} \times t_{\rm p}$, both for model and data representative points. To account for the likely large dispersion of the $\Gamma_* \propto E_{\rm iso,53}^{1/2}$ relation (Hascoet et al. 2013), we also plot sequences corresponding to Γ_0 multiplied or divided by 3. Similarly, in the forward shock scenario we represent sequences where the wind parameter A_* has been multiplied or divided by 3. In some plots this dispersion has little effect, while in some others, especially $[t_{\rm p}, E_{\gamma,\rm iso}]$, it is quite large, but still compatible with the scatter of the data.

6 DISCUSSION AND CONCLUSION

We have addressed in this paper the origin of the plateau phase that is observed in about 50% of the early afterglow light curves observed by *Swift* XRT (Nousek et al. 2006). We have shown that the commonly invoked cause of plateau formation by continuous energy injection into the forward shock leads to an efficiency crisis for the prompt mechanism as soon as the plateau duration exceeds 10^3 seconds.

We have then discussed two alternatives to energy injection,

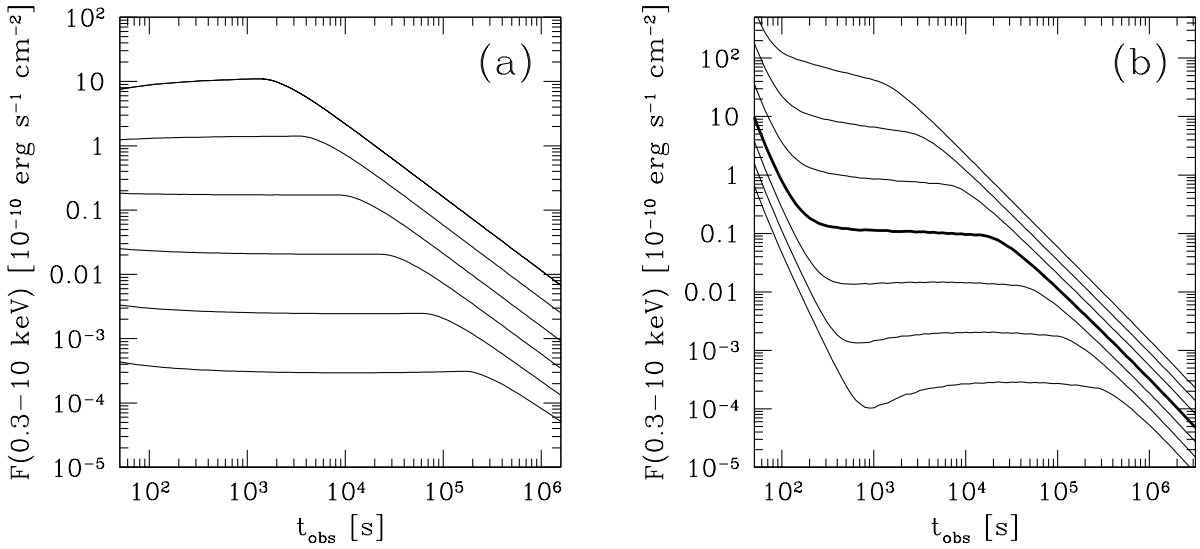

Figure 4. Sequences of X-ray afterglow light curves with plateaus. (a): forward shock scenario with $\epsilon_e \propto n^{-1}$ for $n > n_0 = 15$ cm^{-3}, a wind parameter $A_* = 0.5$ and a gamma-ray efficiency $f_\gamma = 0.2$. The bottom curve corresponds to an energy injected into the forward shock of 8.5×10^{51} erg and the others by successive multiplication of the energy by a factor $F = 2.5$; (b): reverse shock scenario with $\epsilon_e = 0.1$, $\epsilon_B = 0.01$, an external medium of uniform density $n = 1000$ cm^{-3}, a distribution of power in the tail given by Eq. (9) with $q = 8/3$ and $q' = 4/3$. The thick light curve has $E_{\rm H} = E_{\rm T} = 2\,10^{54}$ erg and $\Gamma_* = 16$, while the three others above (resp. below) are obtained by successively multiplying (resp. dividing) the energies by $F = 2.5$ and the Lorentz factors by $F^{1/2}$. In both panels an index $p = 2.2$ for the electron spectrum and a redshift $z = 1$ have been assumed.

the first one still in the context of the forward shock scenario, the second in the more speculative one where the early afterglow is made by a long-lived reverse shock. Within the forward shock scenario a simple way to produce a plateau is to reduce the radiative efficiency of the shock by acting on the microphysics parameter ϵ_e. For a wind external medium a simple dependence of the form $\epsilon_e \propto n^{-1}$ for n larger than a critical density n_0 leads to the formation of a plateau approximately satisfying the prompt-afterglow correlations. The possibility of such a specific behavior of ϵ_e remains to be confirmed but it is striking that playing with only one parameter of the model can account for both the plateau formation and its phenomenology.

In the reverse shock scenario, the shape of the early afterglow is fixed the distribution of injected power $\dot{E}_{\rm T}(\Gamma)$ in the low Γ tail that is crossed by the shock. Using simple power laws for $\dot{E}_{\rm T}(\Gamma)$ we have shown that flat plateaus and correct post-plateau decays can be obtained by adjusting the indices of the power laws. In addition, to satisfy the prompt-afterglow correlations the typical Lorentz factor of the ejecta should increase with burst energy. A relation of the form $\Gamma \propto E_{\gamma,{\rm iso}}^{1/2}$, with a large scatter allowed, provides a reasonable fit of the data. Since the reverse shock is more efficient in a uniform rather than in a wind external medium, the same plateau luminosity can be achieved with 3 times less energy in the tail and we have then only presented results for this former case.

The reverse shock scenario represents a true change of paradigm compared to the standard viewpoint. It has a much larger flexibility in terms of shapes of afterglow light curves. In addition to the capability to produce a plateau it can also account for various accidents such as bumps or steep slopes that are commonly observed (Uhm et al. 2012). We have limited the present study to the X-ray light-curves, but extending the analysis to the visible/radio domains might help to discriminate between the forward and reverse shock scenarii we have considered.

ACKNOWLEDGMENTS

It is a pleasure to thank Raffaella Margutti who kindly sent us her data on the prompt-afterglow correlations. This work has been financially supported by NSF grant AST-1008334 and the Programme National Hautes Energies (PNHE).

REFERENCES

Beloborodov, A. M. 2005, ApJ, 627, 346
Beloborodov, A. M. 2010, MNRAS, 407, 1033
Daigne, F. & Mochkovitch, R. 1998, MNRAS, 296, 275
Dainotti, M. G., Ostrowski, M., & Willingale, R. 2011, MNRAS, 418, 2202
Dainotti, M. G., Petrosian, V., Singal, J., & Ostrowski, M. 2013, ApJ, 774, 157
Drenkhahn, G. & Spruit, H. C. 2002, A&A, 391, 1141
Gehrels, N., Chincarini, G., Giommi, P., et al. 2004, ApJ, 611, 1005
Genet, F., Daigne, F., & Mochkovitch, R. 2007, MNRAS, 381, 732
Ghirlanda, G., Nava, L., Ghisellini, G., et al. 2012, MNRAS, 420, 483
Granot, J., Königl, A., & Piran, T. 2006, MNRAS, 370, 1946
Grupe, D., Nousek, J. A., Veres, P., Zhang, B.-B., & Gehrels, N. 2013, ApJS, 209, 20
Hascoet, R., Beloborodov, A. M., Daigne, F., & Mochkovitch, R. 2013, ArXiv e-prints

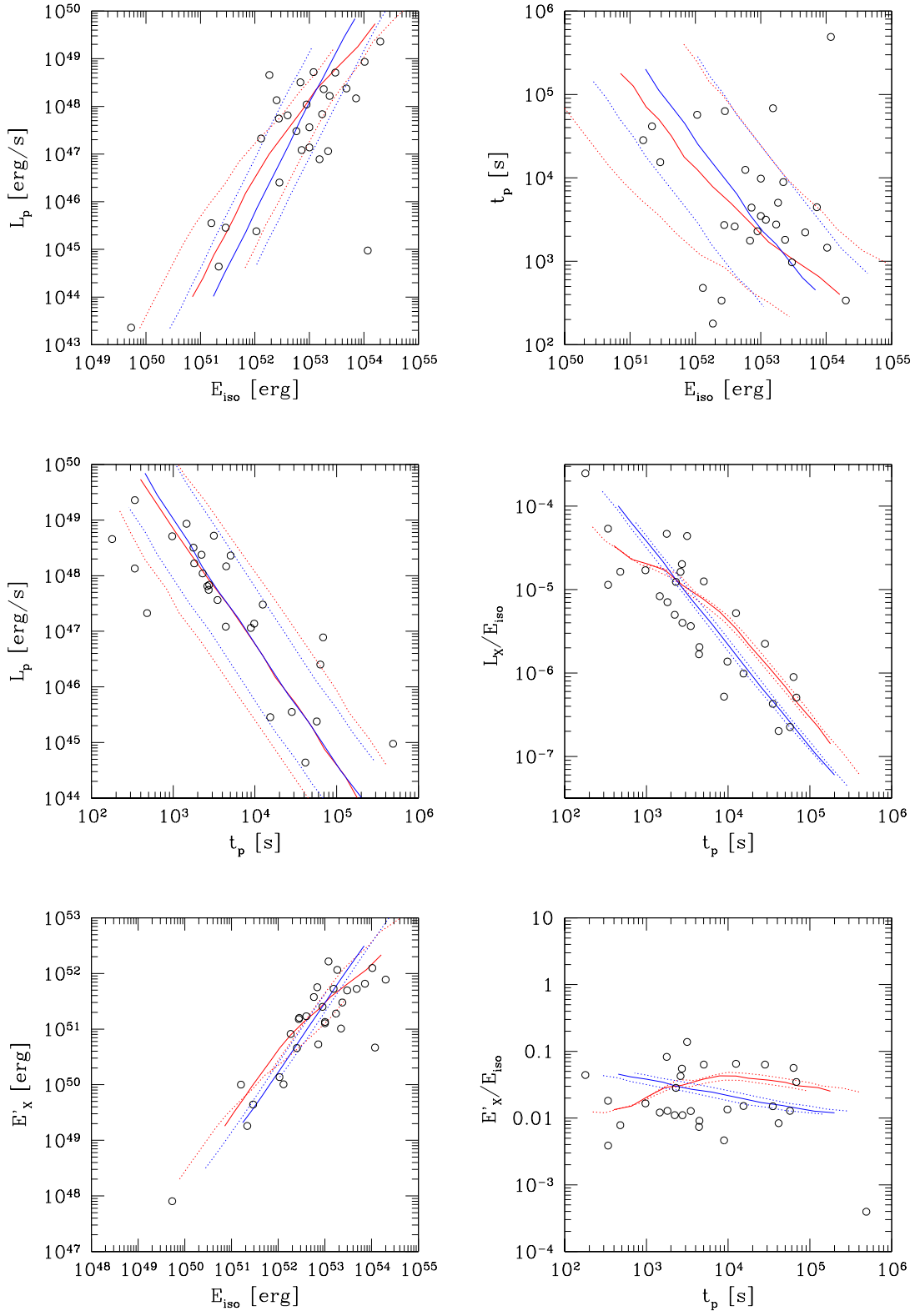

Figure 5. Prompt-afterglow correlations. The blue line correspond to the forward shock case and the red line to the reverse shock case. The blue and red dotted lines respectively illustrate the effects of a factor of 3 dispersion in the wind parameter A_* and in the relation $\Gamma_* \propto E_{\gamma,\rm iso}^{1/2}$ (see text for details).

Hascoët, R., Daigne, F., Mochkovitch, R., & Vennin, V. 2012, MNRAS, 421, 525
Ioka, K., Toma, K., Yamazaki, R., & Nakamura, T. 2006, A&A, 458, 7
Kobayashi, S., Piran, T., & Sari, R. 1997, ApJ, 490, 92
Liang, E.-W., Yi, S.-X., Zhang, J., et al. 2010, ApJ, 725, 2209
Lithwick, Y. & Sari, R. 2001, ApJ, 555, 540
Margutti, R., Zaninoni, E., Bernardini, M. G., et al. 2013, MNRAS, 428, 729
Meszaros, P. & Rees, M. J. 1997, ApJ, 476, 232
Nousek, J. A., Kouveliotou, C., Grupe, D., et al. 2006, ApJ, 642, 389
O'Brien, P. T., Willingale, R., Osborne, J., et al. 2006, ApJ, 647, 1213
Panaitescu, A. & Kumar, P. 2000, ApJ, 543, 66
Rees, M. J. & Meszaros, P. 1994, ApJL, 430, L93
Rees, M. J. & Meszaros, P. 1998, ApJL, 496, L1
Rees, M. J. & Mészáros, P. 2005, ApJ, 628, 847
Rowlinson, A., O'Brien, P. T., Metzger, B. D., Tanvir, N. R., & Levan, A. J. 2013, MNRAS, 430, 1061
Sari, R. & Mészáros, P. 2000, ApJL, 535, L33
Sari, R., Piran, T., & Narayan, R. 1998, ApJL, 497, L17
Shen, R. & Matzner, C. D. 2012, ApJ, 744, 36
Spruit, H. C., Daigne, F., & Drenkhahn, G. 2001, A&A, 369, 694
Uhm, Z. L. & Beloborodov, A. M. 2007, ApJL, 665, L93
Uhm, Z. L., Zhang, B., Hascoët, R., et al. 2012, ApJ, 761, 147
Zhang, B., Fan, Y. Z., Dyks, J., et al. 2006, ApJ, 642, 354
Zhang, B., Liang, E., Page, K. L., et al. 2007, ApJ, 655, 989